

Critical behavior at nematic-to-smectic- A phase transitions for smectic- A_1 and reentrant smectic- A_d phases

K. W. Evans-Lutterodt,* J. W. Chung,* B. M. Ocko,* R. J. Birgeneau,*
C. Chiang,[†] and C. W. Garland[†]

Center for Materials Science and Engineering, Massachusetts Institute of Technology, Cambridge, Massachusetts 02139

E. Chin and J. Goodby

AT&T Bell Laboratories, Murray Hill, New Jersey 07974-2070

Nguyen Huu Tinh

Centre de Recherche Paul Pascal, Domaine Universitaire de Bordeaux I, 33405 Talence, France

(Received 11 February 1987)

We have carried out high-resolution x-ray scattering and heat-capacity studies of the nematic (N)→smectic- A (SmA) transitions in 4'-(4''- n -alkoxybenzyloxy)-4-cyanostilbene with the alkyl chain of length 7 (T7) and 8 (T8). The material T7 exhibits only a single nematic-to-smectic- A_1 transition where the SmA_1 period is commensurate with the molecular length l . T8 exhibits with decreasing temperature the doubly reentrant sequence N - SmA_d - N - SmA_1 where the SmA_d period is incommensurate with $d \sim 1.2l$. For both T7 and T8 we find second-order N - SmA_1 transitions with identical reduced amplitudes and exponents; the critical exponents so obtained are $\gamma = 1.22 \pm 0.06$, $\nu_{\parallel} = 0.69 \pm 0.03$, $\nu_{\perp} = 0.63 \pm 0.03$, and $\alpha = 0.06 \pm 0.06$. These are close, but not identical, to those expected for an ideal XY transition and they give $\nu_{\parallel} + 2\nu_{\perp} + \alpha - 2 = 0.01 \pm 0.15$, in good agreement with anisotropic hyperscaling. The lower N - SmA_d transition in T8 gives $\gamma = 1.53 \pm 0.1$, $\nu_{\parallel} = 0.88 \pm 0.05$, and $\nu_{\perp} = 0.76 \pm 0.05$, in disagreement with all models. The heat capacity associated with this transition is too small to yield a reliable value for the critical exponent α . In the reentrant nematic phase of T8, the SmA_d and SmA_1 fluctuations are essentially independent; the SmA_d fluctuations change over from being SmA -like to SmC -like with decreasing temperature in the reentrant nematic phase.

I. INTRODUCTION

Critical behavior at the nematic (N)–smectic- A (SmA) transition has now been extensively studied in a wide variety of liquid-crystal systems.^{1–3} From these experimental studies a consistent pattern has emerged. The exponents typically are close, but not identical, to those expected for an idealized three-dimensional (3D) XY transition. However, the correlation lengths grow anisotropically, in violation of conventional scaling ideas. Further, the exponents are nonuniversal although they are internally consistent to the extent that various scaling laws are satisfied. These nonuniversal exponents seem to vary in a regular fashion with the nematic temperature range and it has been suggested that the “true” N - SmA exponents would be obtained in systems with very long nematic ranges.^{1,2}

Concurrent with these detailed studies of critical phenomena at the N - SmA transition, it has been discovered that the SmA phase itself is much richer than originally anticipated. Specifically, researchers at Bordeaux and others have synthesized new families of polar smectogenic materials which exhibit phase transitions between distinct SmA phases.^{4,5} These materials and the nature of the different SmA phases they exhibit are themselves extremely interesting and important.^{6–9} Studies of critical phenomena in these materials have now just begun to be re-

ported.¹⁰

In this paper we report high-resolution x-ray scattering and heat-capacity studies of the N - SmA critical behavior in the materials 4'-(4''- n -alkoxybenzyloxy)-4-cyanostilbene with alkyl chain lengths of 7 (T7) and 8 (T8). The molecular structure and the general phase diagram¹¹ for alkyl chain lengths between 7 and 9 are shown in Fig. 1. T7 exhibits the sequence of phases

$$\begin{array}{c} \sim 566 \text{ K} \quad \sim 400 \text{ K} \\ I \rightarrow N \rightarrow SmA_1, \end{array}$$

while T8 exhibits a reentrant sequence

$$\begin{array}{c} \sim 566 \text{ K} \quad \sim 521 \text{ K} \quad \sim 412 \text{ K} \quad \sim 367 \text{ K} \\ I \rightarrow N \rightarrow SmA_d \rightarrow N \rightarrow SmA_1. \end{array}$$

For T7 one has $T_{NA}/T_{NI} = 0.7$ compared with, for example, 0.93 in N -(4- n -butyloxybenzylidene)-4'- n -heptylaniline (40.7) which has previously been considered to show characteristic N - SmA critical behavior. Clearly the very long nematic range in T7 will allow one to test the conjecture of Ref. 1 that in such materials one would observe true N - SmA exponents. We should note, however, that Chan *et al.*¹⁰ have already found exponents for the N - SmA_d transition in 4- n -hexylphenyl-4'-(4''-cyanobenzoyloxy)benzoate (DB6) where $T_{NA}/T_{NI} = 0.82$ which do not follow the suggested trend. Chan *et al.*¹⁰ have also studied the N - SmA_1 transition in mixtures of DB6 and terephthalylidene-bis-butylaniline (TBBA) but the inter-

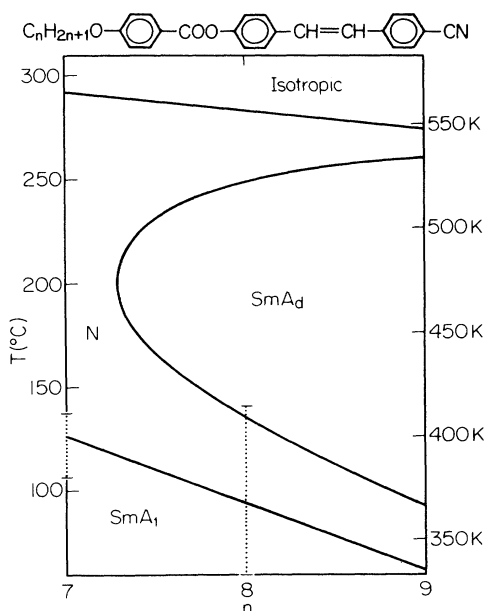


FIG. 1. Phase diagram from Ref. 11 of T_n (cyanoalkylterphenyl) compounds and their mixtures. Data were taken on T7 and T8 over the range of temperatures indicated by the dotted vertical lines. The structure of a T_n molecule is shown at the top.

pretation of the exponents obtained in those experiments is complicated by the presence of a nearby N - SmA_1 - SmA_2 multicritical point as well as possible Fisher renormalization effects.

Studies of T8 are of interest for two reasons. First, one can compare the critical behavior for N - SmA_1 and N - SmA_d transitions in the same material. Second, the reentrancy itself is quite interesting.^{6,7,12} Qualitative studies of the smectic fluctuations in the reentrant nematic phase have been reported by Hardouin and Levelut.¹³ As we shall show, a more detailed quantitative study reveals new and interesting behavior.

The format of this paper is as follows. The heat capacity and x-ray experimental results and analyses are reported in Sec. II. A brief discussion and conclusions are given in Sec. III.

II. EXPERIMENTAL RESULTS AND ANALYSIS

A. Material preparation

The compounds T7 and T8 were prepared by a classical seven-step synthetic procedure from 4-bromophenyl-acetic acid. Initially, this acid was chlorinated with thionyl chloride to give the corresponding acid chloride. This was reacted with anisole in a Friedel-Crafts acylation reaction to give 4'-bromobenzyl-4-methoxyphenone in good yield. The product was demethylated in the presence of hydrobromic acid to give 4'-bromobenzyl-4'-hydroxyphenone. This phenone was reduced with lithium aluminum hydride to the corresponding alcohol, which in turn

was dehydrated with formic acid yielding 4-bromo-4'-stilbene. The resulting stilbene was cyanated with cuprous cyanide, thereby producing 4-cyano-4'-hydroxystilbene, which in turn was esterified with the appropriate acid chloride to give the desired 4'-(4''- n -alkoxybenzoyloxy)-4-cyanostilbene.

The purities of the products were determined at each stage by reverse-phase high-performance liquid chromatography over octadecylsiloxane using acetonitrile as the eluant. Detection of the eluting fractions was made spectroscopically at 254 nm. The purities of the final products were found to be better than 99%, with no trace of the cis isomer being present. The structures of the products of each stage of the synthesis were confirmed by infrared, NMR, and mass spectral analysis.

B. Heat capacity

The heat-capacity measurements on T7 and T8 were carried out with a computer-controlled calorimeter, the operation of which is described elsewhere.¹⁴ The observed heat capacity $C_p(\text{obs})$ corresponded to the total heat capacity of a sealed silver cell containing about 75 mg of liquid crystal. The values of the liquid-crystal specific heat (heat capacity per gram) were obtained from

$$C_p = [C_p(\text{obs}) - C_p(\text{empty cell})] / m, \quad (1)$$

where $C_p(\text{empty cell})$ is the measured heat capacity of the empty silver cell plus heater, thermistor, and electrical leads, and m is the mass of the liquid-crystal sample. $C_p(\text{empty cell})$ is roughly one-half $C_p(\text{obs})$ and it exhibits a very weak (linear) temperature dependence over the entire investigated range.

The specific-heat variation for T8 over a wide temperature range (335–415 K) has been reported elsewhere.¹⁵ The overall C_p behavior (see Fig. 5 of Ref. 16) exhibits a noncritical background variation that is linear in T as expected and has two peaks associated with the N - SmA_d and N - SmA_1 transitions. The N - SmA_d specific-heat peak is very small, and the value of $T_c(N$ - $SmA_d)$ decreased

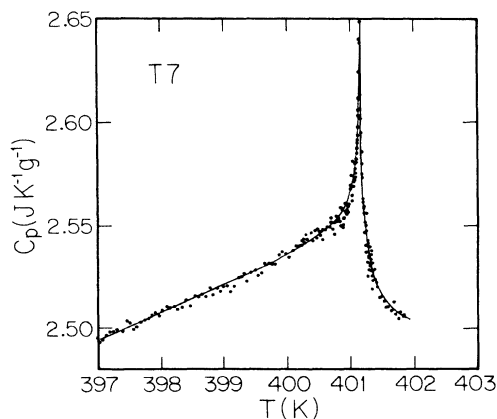


FIG. 2. Specific heat of T7 near the N - SmA_1 transition. The smooth curve represents a fit to the data with Eq. (2) using the parameters of fit 4, for which $\alpha = 0.047$.

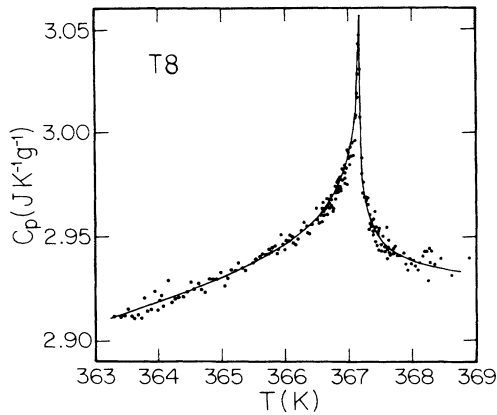


FIG. 3. Specific heat of T8 near the N - SmA_1 transition. The smooth curve represents a fit to the data with Eq. (2) using the parameters of fit 2, for which $\alpha=0.066$.

slowly with time. Thus the $C_p(N-SmA_d)$ data are not suitable for analysis in terms of critical exponents and will not be discussed here.

Detailed measurements of C_p in the vicinity of the N - SmA_1 transition for T7 and T8 are shown in Figs. 2 and 3, respectively. These were carried out on material synthesized in Bordeaux. It is quite clear that the size and shape of these two N - SmA_1 specific-heat peaks are very similar, a conclusion that is confirmed by our quantitative analysis in terms of power-law singularities.

The critical thermal analysis of our C_p values was carried out using a scaling form ($\alpha^+=\alpha^-$ and $B^+=B^-$) which allowed for the inclusion of corrections-to-scaling terms,

$$C_p^\pm = A^\pm |t|^{-\alpha}(1 + D^\pm |t|^{0.5}) + B + E(T - T_c), \quad (2)$$

where t is the reduced temperature $(T - T_c)/T_c$, and the superscript \pm denotes $T > T_c$ or $T < T_c$. Least-squares fits were carried out with both a simple power law ($D^+ = D^- = 0$) and the corrections-to-scaling form with the exponent fixed at 0.5. The least-squares values of the fitting parameters are given in Table I. In the case of T8, the fit is not sensitive to the inclusion of corrections-to-scaling terms, and good fits are obtained for a critical exponent $\alpha \approx 0.07$. In the case of T7, the fit is rather poor for a simple power law, but good fits can be achieved when corrections-to-scaling terms are included. With $D^\pm \neq 0$, $\alpha = 0.047$ is obtained when α is taken to be a free parameter. A fit of equal quality can also be achieved

when α is fixed at 0.066. The minimum in χ^2_ν is rather broad for both T7 and T8, and the uncertainty in the critical exponent α is estimated to be ± 0.06 in both cases. This is a reflection of the fact that the magnitude of the thermal-fluctuation specific-heat-peak is fairly small ($\sim 6\%$) relative to the noncritical background.

In summary, the $C_p(N-SmA_1)$ peaks in T7 and T8 are quite similar in size and shape. Both peaks are best described as very weak divergences ($\alpha \approx 0.06 \pm 0.06$), but a sharp finite cusp such as that predicted for the XY model ($\alpha_{XY} = -0.007$) (Ref. 16) cannot be ruled out.

C. X-ray scattering results

The x-ray scattering experiments were carried out using Cu $K\alpha$ x rays from a Rigaku 12-kW rotating-anode source operating at 8 kW. Two different spectrometer configurations were used, one employing perfect Si(111) and the other perfect Ge(111) as monochromators and analyzers. The longitudinal resolutions so obtained were $2.5 \times 10^{-4} \text{ \AA}^{-1}$ and $4.6 \times 10^{-4} \text{ \AA}^{-1}$ full width at half maximum (FWHM), respectively. The transverse in-plane resolution was essentially perfect. The transverse out-of-plane resolution, which was determined simply by slits, was 0.05 \AA^{-1} FWHM. The samples were placed in beryllium cells in a two-stage temperature controlled oven; the temperature was stable to better than $\pm 0.002 \text{ K}$ for periods of more than one hour.

We discuss first the x-ray measurements in T7; here the Si spectrometer configuration was used. The results shown in Fig. 4 were taken on material prepared in Bordeaux. The oven used in these measurements could not be heated above 410 K; thus we only obtained data within 10 K of $T_c = 400.55 \text{ K}$. The x-ray data in the nematic phase near the N - SmA_1 phase boundary are dominated by a single peak centered about $\mathbf{q} = (0, 0, 0.2119) \text{ \AA}^{-1}$. This corresponds to a smectic lattice spacing of 29.65 \AA , close to, but slightly less than, the length of $\sim 30.4 \text{ \AA}$ for a fully extended T7 molecule.¹⁷ It is evident from Fig. 4 that the longitudinal scan is slightly asymmetric with weak excess scattering on the low- q_{\parallel} side. Comparison with data in T8 suggests that this excess scattering arises from local fluctuations into the SmA_d state. Otherwise, the overall scattering is very much like that at other N - SmA transitions studied previously. We will postpone our discussion of the quantitative analysis of these data until after we present the results in T8.

Preliminary experiments on T8 were performed on samples prepared at Bordeaux; more detailed studies were

TABLE I. Least-squares parameter values obtained on fitting the N - SmA_1 specific heat with Eq. (1). The value of T_c is 401.170 K for T7 and 367.163 K for T8. Parentheses indicate that a parameter was held constant at the indicated value.

Fit	Material	α	A^+	A^-	D^+	D^-	B	E	χ^2_ν
1	T8	0.075	0.1266	0.1421	(0)	(0)	2.733	0.0053	1.26
2	T8	0.066	0.1455	0.1657	0.217	-0.387	2.714	0.0045	1.12
3	T7	0.016	1.0753	1.1053	(0)	(0)	1.317	0.0006	3.00
4	T7	0.047	0.3453	0.3522	-0.473	2.464	2.034	0.0207	1.16
5	T7	(0.066)	0.2013	0.2067	-1.007	3.359	2.198	0.0190	1.16

carried out on T8 samples synthesized at Bell Laboratories. The results are sample independent as one would expect. We found that the phase-transition temperatures for T8 when contained in a glass holder were stable in time; however, the mosaicity was poor. When T8 was placed in a beryllium cell, T_{NA_d} and T_{NA_1} both decreased markedly over the period of several days. However, they stabilized at $T_{NA_d}=401.41$ K and $T_{NA_1}=361.17$ K and were then independent of time for at least one month. This rapid diminution in T_c may be related to a change in the cis- and trans-distribution since all-trans material exhibits lower T_c 's. We do not believe that any of our results are affected by this lowering of the phase-transition temperatures.¹⁸

Figure 5 shows a series of scans in T8 in the middle region of the reentrant nematic (RN) phase. The data cover the region from near the N - SmA_d boundary to near the N - SmA_1 boundary. At the N - SmA_d boundary the scattering is dominated by a peak at $\mathbf{q}=(0,0,0.1745)$ \AA^{-1} while at the N - SmA_1 boundary there is a prominent peak at $\mathbf{q}=(0,0,0.2056)$ \AA^{-1} . These correspond to layer spacings of $l_d=36.01$ \AA and $l_1=30.56$ \AA , respectively. Thus the lower smectic phase is indeed a monolayer smectic A_1 while the upper smectic phase is incommensurate SmA_d with $d \simeq 1.18l$. Note that the SmA_d spacing is much closer to the monolayer value than the bilayer spacing; in materials such as DB6 $l_d \simeq 1.9l_1$ and this changes the nature of the competing states and the concomitant phase diagram completely.¹⁰ Survey scans were also carried out along $(0,0,q_{||})$ over a wide range of $q_{||}$. No other scattering with a relative intensity greater than 10^{-3} was found.

At each temperature a longitudinal scan along $(0,0,q_{||})$

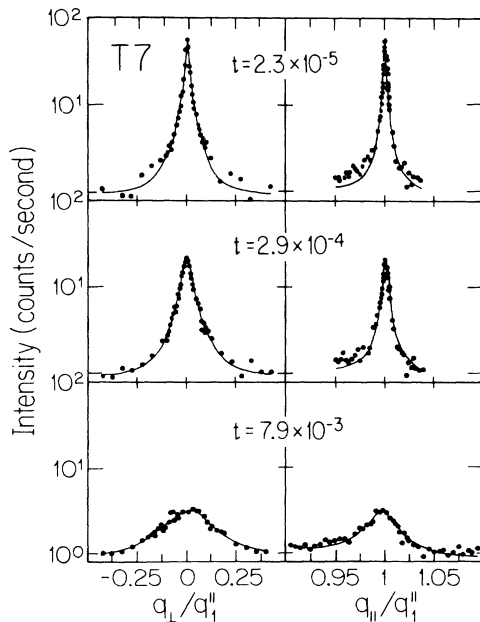


FIG. 4. Transverse and longitudinal x-ray scans in T7 at a series of reduced temperatures t . The solid lines are the results of least-squares fits of Eq. (3) convolved with the instrumental resolution function.

and transverse scans along $(q_{\perp},0,0.848)$ and $(q_{\perp},0,0.98)$ (measured in units of $q_{||}^{\parallel}=0.2056$ \AA^{-1}) were performed. For $T=386.32$ K and above only low statistics transverse scans along $(q_{\perp},0,1)$ were taken; these showed a broad, temperature-dependent peak centered at $(0,0,1)$. These scans are not shown in Fig. 5. It is evident qualitatively that in the reentrant nematic phase there is a gradual cross over from dominant SmA_d to dominant SmA_1 fluctuations with decreasing temperature as noted previously by Hardouin and Levelut.¹³ However, the fluctuations appear to exist independently of each other. This is most evident at the intermediate temperatures. This illustrates

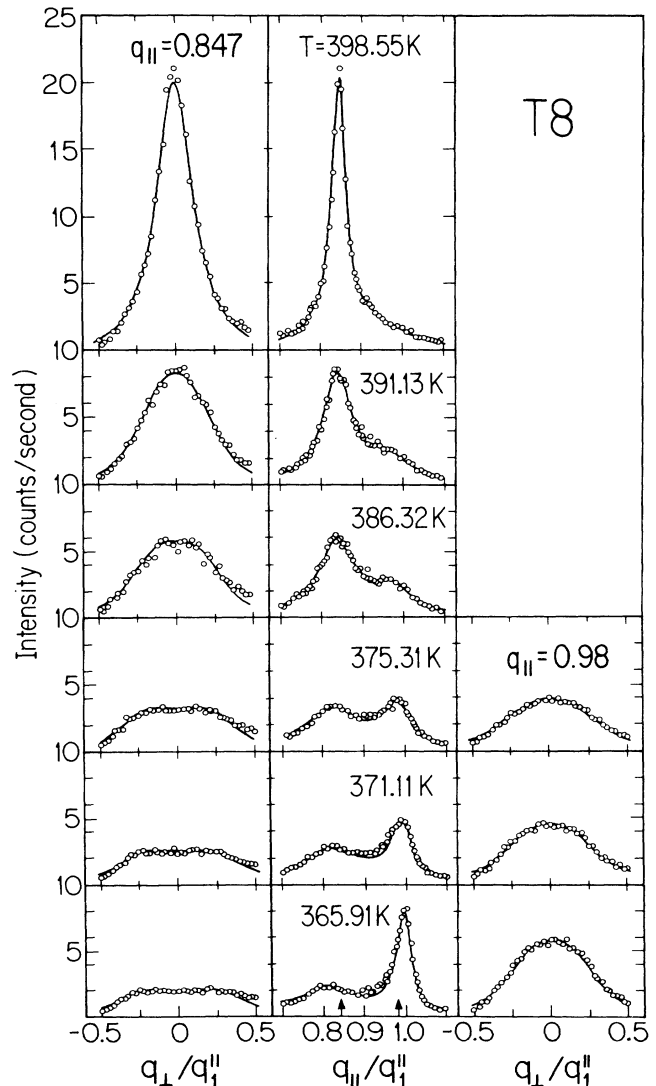


FIG. 5. Transverse and longitudinal x-ray scans in T8 at the indicated temperatures. The left-hand column corresponds to transverse scans along $(q_{\perp},0,0.847)$ while the right-hand column displays data for scans along $(q_{\perp},0,0.98)$. The independent SmA_d and SmA_1 fluctuations are manifest, especially for the middle panels. The solid lines are the results of fits to Eq. (3) and (5) as discussed in the text.

dramatically that the $\text{Sm}A_d$ and $\text{Sm}A_1$ states compete with each other; presumably it is this competition which drives the reentrancy.^{6,7,12} We should note that an alternative possibility was that the $\text{Sm}A_d$ phase and its concomitant fluctuations would simply evolve continuously into the $\text{Sm}A_1$ phase;¹⁹ such a scenario might or might not involve reentrancy. One novel feature which is evident from the left-hand column of Fig. 5 is that with decreasing temperature the $\text{Sm}A_d$ fluctuations go from being A -like to being C -like. This implies that a $\text{Sm}A_d$ - $\text{Sm}C_d$ transition occurs within the correlated droplets in the RN phase.²⁰ In order to discuss these results quantitatively it is necessary to carry out a detailed line-shape analysis of the measured profiles. We therefore proceed to discuss our fits.

$$\xi_1^2 = \begin{cases} \frac{2D_1}{-C_1 + (C_1^2 + 4D_1)^{1/2}}, & C_1 > 0 \\ \frac{2D_1^2}{\left[-C_1 + \left[C_1^2 + 4D_1 \left(1 - \frac{C_1^2}{2D_1} \right) \right]^{1/2} \right]^{1/2} - (-C_1)^{1/2}}, & C_1 < 0. \end{cases} \quad (4a)$$

(4b)

Note that for $C_1 \gg D_1^{1/2}$, $\xi_1^2 = C_1$ as usual and for $C_1 = 0$, $\xi_1^2 = D_1^{1/2}$. The data in Fig. 5 suggest that the $\text{Sm}A_d$ and $\text{Sm}A_1$ fluctuations are independent. Thus to analyze the T8 data in the crossover region we assume

$$S(\mathbf{q}) = S_1(\mathbf{q}) + S_d(\mathbf{q}) \quad (5)$$

with $q_\alpha^\parallel = q_1^\parallel$ and q_α^\perp , respectively; these q vectors are treated as adjustable parameters.

Before discussing the critical behavior we first consider the general evolution of the profiles in the RN phase in T8. The solid lines in Fig. 5 are the results of the fits to Eqs. (3) and (5). Clearly the model describes the measurements quite well. (The slight disagreement for $q_\perp \approx 0.5$ in the left-hand column is an artifact caused by the fringe field from the magnet influencing the detector; this was discovered after the measurements were completed.) There is, of course, an extraordinarily large number of adjustable parameters: σ , ξ_1 , C_1 , D_1 , and q_α^\parallel for each peak. Only in the crossover region are all ten parameters well determined.

Parameters derived from the fits are shown in Figs. 6–8. The smectic susceptibilities and the longitudinal correlation lengths are shown in Fig. 6. The crossover from dominant $\text{Sm}A_d$ to $\text{Sm}A_1$ fluctuations is dramatically illustrated by these data. As noted above, the $\text{Sm}A_d$ fluctuations go from being A -like to C -like with decreasing temperature. In the line-shape fits this is signaled by C_1 changing sign. When C_1 is less than 0 but small the mean tilt is proportional to the transverse wave vector $q_1^0 = (-C_1/2D_1)^{1/2}$. The results for q_1 are shown in Fig. 7. It is evident that q_1^0 arises from zero quasicontinuously for temperatures below about 387 K; indeed the data are

D. X-ray line-shape analysis

Previous experiments have shown that both $\text{Sm}A$ and $\text{Sm}C$ fluctuations in nematic phases are well described by the form^{20,21}

$$S(\mathbf{q})_\alpha = \frac{\sigma}{1 + \xi_\parallel^2 (q_\parallel - q_\alpha^\parallel)^2 + C_1 q_\perp^2 + D_1 q_\perp^4}. \quad (3)$$

For $\text{Sm}A$ fluctuations $C_1 > 0$, while for $\text{Sm}C$ fluctuations $C_1 < 0$ and one has a torus of scattering centered about the transverse wave vector $q_1^0 = (-C_1/2D_1)^{1/2}$. As discussed by Martinez-Miranda *et al.*, the transverse correlation length is conveniently defined as the inverse half width and half maximum;²⁰ with this definition

quite reminiscent of those at an ordinary $\text{Sm}A$ - $\text{Sm}C$ transition.²² The solid line is the power law $(386.39 - T)^{0.30}$ which describes the data well. More detailed experiments are required to establish the validity of this power-law

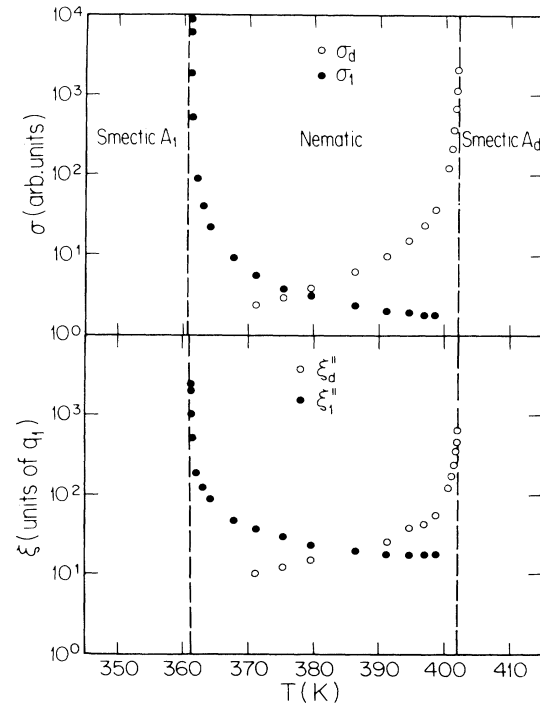


FIG. 6. Smectic susceptibility vs temperature in the reentrant nematic phase in T8 for the $\text{Sm}A_d$ and $\text{Sm}A_1$ fluctuations.

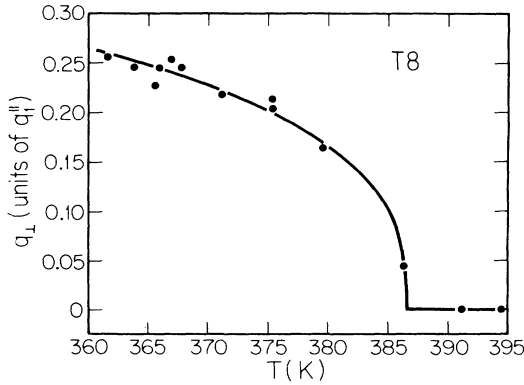


FIG. 7. Transverse wave vector $q_{\perp}^0 = (-C_{\perp}/2D_{\perp})^{1/2}$ in T8 for the tiled SmA_d fluctuations. The solid line is a simple power law with exponent 0.30.

description.

The q_{\parallel} vectors for the SmA_d and SmA_1 scattering are shown in Fig. 8. The squares are the data of Hardouin and Levelut¹³ in the SmA_d phase; all other data are from this study. The apparent discontinuity for q_{\parallel}^0 at the phase boundary is an artifact of combining data from different laboratories on different samples. Specifically, we find that q_{\parallel}^0 varies smoothly through the $N-SmA_d$ phase boundary. We note that dq_{\parallel}^0/dT changes sign between the SmA_d and RN phases. Further, q_{\parallel}^0 decreases smoothly through the “ $A-C$ transition” while the peak q vector, $q_d = 2\pi/l_d$, increases below the putative transition as expected since the layer spacing should decrease with increasing tilt.²² Finally, we note that the monolayer q vector q_{\parallel} increases by about 5% across the RN phase. This corresponds to a decrease in the SmA_1 layer spacing by about 1.5 Å from the $N-SmA_d$ to the $N-SmA_1$ phase boundaries.

E. X-ray critical behavior

The data in the critical region were analyzed using Eq. (3) since $D_{\perp}^{1/2}/C_{\perp}$ is always quite small; then to a very

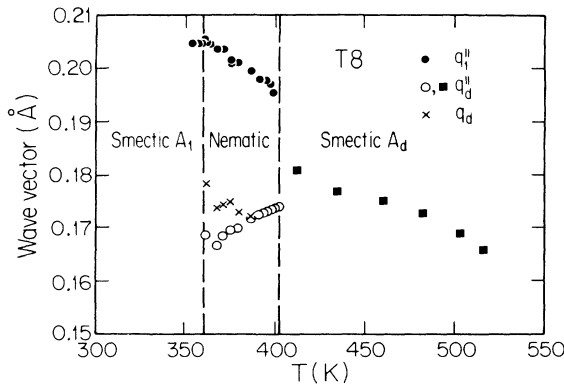


FIG. 8. Peak wave vector vs temperature in T8; the solid squares are from Hardouin and Levelut (Ref. 13). The other points, which are primarily in the RN phase, are from this work. q_d represents the magnitude of the wave vector at $(q_{\perp}^0, 0, q_{\parallel}^0)$ when the SmA_d fluctuations are tilted.

good approximation $\xi_{\perp}^2 = C_{\perp}$. In the critical region, that is, within $t = 10^{-2}$, the relevant divergent susceptibility completely dominated the scattering so that one could not reasonably fit all ten parameters in Eq. (4). For T7 the diffuse scattering on the low- q_{\parallel} side which was always very weak was incorporated into a sloping background which was independent of temperature. For T8 at the $N-SmA_1$ transition the data were cut off on the low- q side to eliminate the SmA_d fluctuation scattering while a complementary cut off was used for the $N-SmA_d$ transition.

Long range order is signaled by a sudden appearance of mosaicity which in turn reflects itself as an anomaly in the temperature dependence of the peak intensity. Using this technique T_c could be located to within ± 0.002 K in a measuring time of about three minutes. The instantaneous T_c was monitored using the technique during the experiments. For T7 it was found that T_c decreased by 0.002 K per hour; since scans at a given temperature took about 20 minutes this constituted a negligible correction for data at a fixed temperature. The data overall were, however, corrected for this drift in T_c . For T8 no such correction was required.

The smectic susceptibility, longitudinal and transverse correlation lengths for the $N-SmA_1$ transitions in T7 and T8 are shown in Figs. 9 and 10, respectively. For these plots T_c was fixed at the value determined experimentally. Allowing T_c to vary within reasonable limits has no effect on the plots. It is evident that in T7 and T8 each of σ , ξ_{\parallel} and ξ_{\perp} exhibit single power law behavior over the complete reduced temperature range from $\sim 5 \times 10^{-5}$ to 2×10^{-2} . Remarkably, $\xi_{\parallel} q_{\parallel}^0$ and $\xi_{\perp} q_{\perp}^0$ are identical in T7 and T8 over the complete temperature range. The ratio of lengths $\xi_{\parallel}/\xi_{\perp}$ and the fourth-order coefficient, defined as $C = D_{\perp}/C_{\perp}^2$, are shown in Fig. 11; the mean length ratio is 13.5, about twice the bare molecular ratio, and it evolves by only $\sim 20\%$ over more than two decades in reduced temperature. Thus the $N-SmA_1$ transitions in T7 and T8 are nearly isotropic, in contrast to many previously studied $N-SmA$ transitions.^{1,2} We note that the fourth-order term is negligible except for reduced temperatures of $\sim 10^{-2}$.

Explicit fits of single power laws to the data in Figs. 9

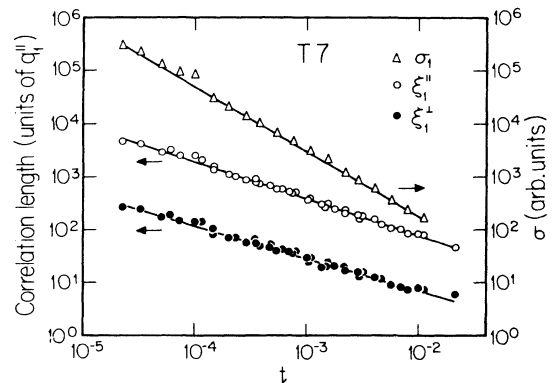


FIG. 9. Smectic susceptibility, longitudinal and transverse correlation lengths at the $N-SmA_1$ transition in T7. The solid lines are the single power laws, Eq. (6).

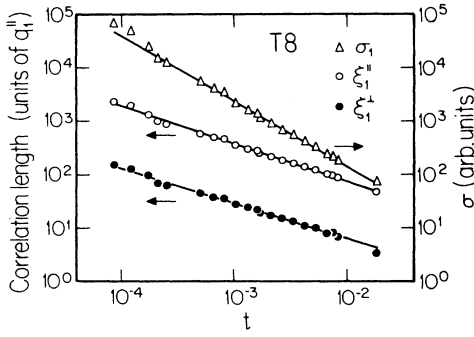


FIG. 10. Smectic susceptibility, longitudinal and transverse correlation lengths at the N - SmA_1 transition in T8. The solid lines are the single power laws, Eq. (7).

and 10 give, for T7,

$$\begin{aligned} \sigma &= \text{const} \times t^{-1.22 \pm 0.06}, \\ \xi_{||} q_1^{\parallel} &= (3.23 \pm 0.1) t^{-0.69 \pm 0.03}, \\ \xi_{\perp} q_1^{\perp} &= (0.41 \pm 0.05) t^{-0.61 \pm 0.03}; \end{aligned} \quad (6)$$

and, for T8,

$$\begin{aligned} \sigma &= \text{const} \times t^{-1.22 \pm 0.06}, \\ \xi_{||} q_1^{\parallel} &= (3.14 \pm 0.1) t^{-0.70 \pm 0.03}, \\ \xi_{\perp} q_1^{\perp} &= (0.31 \pm 0.03) t^{-0.65 \pm 0.03}. \end{aligned} \quad (7)$$

The mean N - SmA_1 exponents then are $\gamma = 1.22 \pm 0.06$, $\nu_{||} = 0.69 \pm 0.03$, and $\nu_{\perp} = 0.63 \pm 0.03$.

The data for the N - SmA_d transition in T8 are shown in Fig. 12. The circles and triangles correspond to data tak-

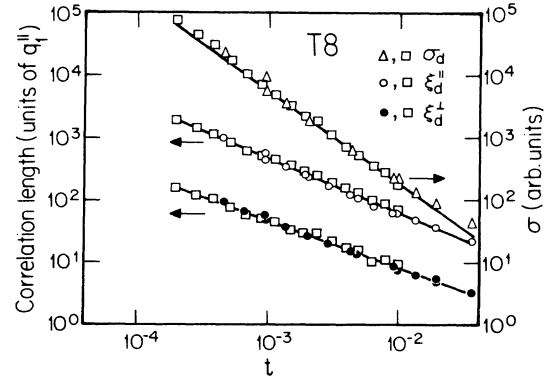


FIG. 12. Smectic susceptibility, longitudinal and transverse correlation lengths at the N - SmA_d transition in T8. The solid lines are the single power laws, Eq. (8). The open squares are data taken with the Si(111) spectrometer configuration; the others are from our experiment using the Ge(111) spectrometer configuration.

en with the Ge(111) spectrometer while the open squares are data taken with the Si(111) configuration. The good absolute agreement between these two experiments verifies the deconvolution procedure. The correlation length at a given reduced temperature is much larger than that at the N - SmA_1 transitions so it was only possible to obtain data down to a reduced temperature $t = 2 \times 10^{-4}$. Again the data are well described by single power laws with, for T8 (N - SmA_d),

$$\begin{aligned} \sigma &= (\text{const}) t^{-1.53 \pm 0.1}, \\ \xi_{||} q_1^{\parallel} &= (1.11 \pm 0.1) t^{-0.88 \pm 0.04}, \\ \xi_{\perp} q_1^{\perp} &= (0.25 \pm 0.02) t^{-0.76 \pm 0.04}. \end{aligned} \quad (8)$$

The exponents $\gamma = 1.53 \pm 0.1$, $\nu_{||} = 0.88 \pm 0.04$, and $\nu_{\perp} = 0.76 \pm 0.04$ are all much larger than those obtained at the N - SmA_1 transitions.

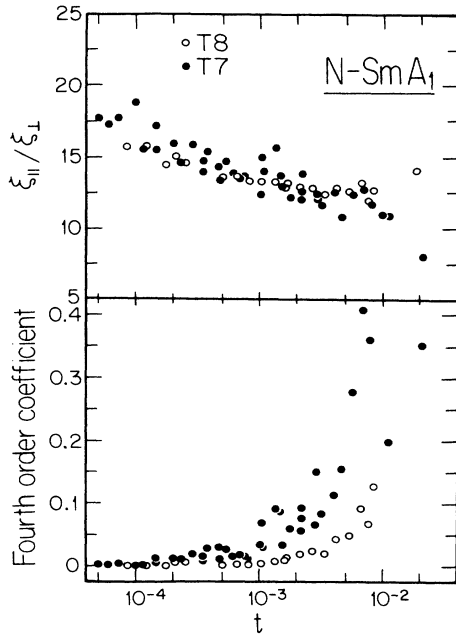


FIG. 11. Length ratio $\xi_{||}/\xi_{\perp}$ and fourth-order coefficient $C(D_1 = C\xi_1^4)$ at the N - SmA_1 transitions in T7 and T8.

TABLE II. Critical parameters in various N - SmA_1 transitions.

Material	T_{NA}/T_{NI}	γ^a	$\nu_{ }^b$	ν_{\perp}^b	α^a
T8	0.66	1.22	0.70	0.65	0.07
T7	0.71	1.22	0.69	0.61	0.05
4O.7 ^c	0.926	1.46	0.78	0.65	-0.03
8S5 ^d	0.936	1.53	0.83	0.68	0
4O.8 ^e	0.958	1.31	0.70	0.57	0.15
XY model ^f		1.32	0.67	0.67	-0.01

^aThe errors are typically ± 0.06 .

^bThe errors are typically ± 0.03 .

^cReference 1.

^dReference 27; 8S5 is an abbreviation for 4-*n*-octyloxy-4'-(*n*-pentyl)phenyl thiolbenzoate.

^eReference 26; 4O.8 is an abbreviation for *N*-(4-*n*-butyloxybenzylidene)-4'-*n*-octylaniline. Note that 4O.7, 8S5, and 4O.8 are all nonpolar, in contrast to T7 and T8.

^fReference 16.

TABLE III. Critical parameters in various N -Sm A_d transitions.

Material	T_{NA}/T_{NI}	γ^a	ν_{\parallel}^b	ν_{\perp}^b	α^a
T8	0.74	1.53	0.88	0.76	
DB6 ^c	0.82	1.29	0.67	0.52	
CBOOA ^d	0.94	1.30	0.70	0.62	0.15
8OCB ^e	0.963	1.32	0.71	0.58	0.2
XY model ^f		1.32	0.67	0.67	-0.01

^aThe errors are typically ± 0.06 .

^bThe errors are typically ± 0.03 .

^cReference 10.

^dReference 23; CBOOA is an abbreviation for N -(*p*-cyanobenzylidene)-*p*'-octyloxyaniline.

^eReference 12; 8OCB is an abbreviation for 4-cyano-4'-(*n*-octyloxy)biphenyl.

^fReference 16.

III. DISCUSSION AND CONCLUSIONS

The results of these experiments and selected previous measurements on N -Sm A transition are given in Tables II and III. As we noted in Sec. I, previous studies of the N -Sm A transition have indicated nonuniversal behavior with anisotropic exponents.^{1,2} Nevertheless, various scaling laws are satisfied. Unfortunately, there is so far no information on the nematic elastic constants so we cannot test the predicted relationships³ between K_2, K_3 and ξ_{\parallel} and ξ_{\perp} nor can we estimate the crossover region of Lubensky *et al.*²⁴ for ξ_{\perp} . We can, however, test the relationship between the heat capacity and the correlated volume. Specifically, on general grounds one expects

$$C_p t^2 \xi_{\parallel} \xi_{\perp}^2 = \text{const} . \quad (9)$$

This leads to the anisotropic hyperscaling scaling relation

$$\nu_{\parallel} + 2\nu_{\perp} + \alpha - 2 = 0 . \quad (10)$$

From Table II for T7 and T8 we have, for T7,

$$\nu_{\parallel} + 2\nu_{\perp} + \alpha - 2 = 0.04 \pm 0.015 ,$$

and, for T8,

$$\nu_{\parallel} + 2\nu_{\perp} + \alpha - 2 = -0.07 \pm 0.15 .$$

Thus anisotropic hyperscaling is indeed well obeyed.

Equation (9) also provides a restriction on the absolute lengths for C_p to be observable. We show in Fig. 13 the measured longitudinal correlation lengths in various materials. The magnitudes of the heat-capacity peak in T7

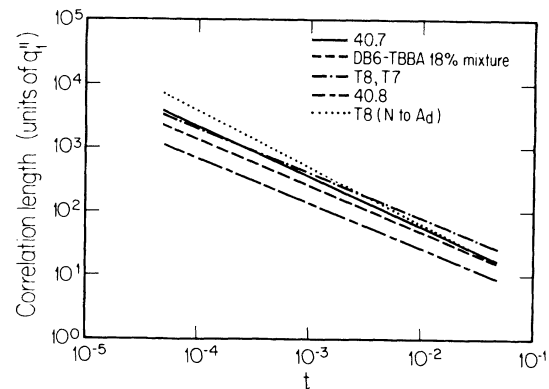


FIG. 13. Longitudinal correlation lengths in units of the peak wave vector q_0^{\parallel} at the N -Sm A transition in various materials. The data are from 40.7, Ref. 1; DB6-TBBA, Ref. 10; T8, T7, this work; 40.8, Ref. 26; T8(N -Sm A_d), this work.

and T8 are indeed consistent with the data in Fig. 13 and Eq. (9).

The situation vis-a-vis the critical exponents themselves is much less satisfactory. For T_{NA}/T_{NI} near unity one expects crossover to tricritical behavior² ($\gamma=1$, $\nu_{\parallel}=\nu_{\perp}=0.5$, $\alpha=0.5$) and this is indeed observed. However, for smaller T_{NA}/T_{NI} previous N -Sm A_1 and N -Sm A_d investigations seemed to show a trend towards larger values^{1,2} of γ , ν_{\parallel} , ν_{\perp} , with $\gamma \simeq 1.5$, $\nu_{\parallel} \simeq 0.8$, $\nu_{\perp} \simeq 0.65$. This trend is explicitly violated by the N -Sm A_1 transitions in T7 and T8 reported here as well as the N -Sm A_d transition in DB6 studied by Chan *et al.*¹⁰ Indeed, in T7 and T8 the measured exponents are quite close to those expected for a simple XY transition as originally predicted by de Gennes.²⁵ On the other hand, the N -Sm A_d transition in T8 exhibits values close to those given above for γ , ν_{\parallel} , and ν_{\perp} . Clearly there is some hidden variable causing this nonuniversal behavior which is not made manifest by Tables II and III. We have no satisfactory explanation for this conundrum.

ACKNOWLEDGMENTS

We acknowledge gratefully illuminating discussions with A. N. Berker, D. L. Johnson, J. D. Litster, and T. C. Lubensky. This work was supported by the National Science Foundation, Materials Research Laboratory Program, under Grant No. DMR84-18718. The x-ray work reported here constitutes a thesis submitted by one of us (K.W.E.-L.) for the S.B. degree in Physics and Electrical Engineering at M.I.T.

*Also at Department of Physics, Massachusetts Institute of Technology, Cambridge, MA 02139.

†Also at Department of Chemistry, Massachusetts Institute of Technology, Cambridge, MA 02139.

¹C. W. Garland, M. Meichle, B. M. Ocko, A. R. Kortan, C. R. Safinya, L. J. Yu, J. D. Litster, and R. J. Birgeneau, Phys. Rev. A **27**, 3234 (1983) and references therein.

²B. M. Ocko, R. J. Birgeneau, and J. D. Litster, Z. Phys. B **62**,

487 (1986); J. Thoen, H. Marynissen, and W. Van Dael, Phys. Rev. Lett. **52**, 204 (1984).

³S. Sprunt, L. Solomon, and J. D. Litster, Phys. Rev. Lett. **53**, 1923 (1984); C. Gooden, R. Mahmood, D. Brisbin, A. Baldwin, D. L. Johnson, and M. E. Neubert, Phys. Rev. Lett. **54**, 1034 (1985).

⁴For a review, see F. Hardouin, A. M. Levelut, M. F. Achard, and G. Sigaud, J. Chim. Phys. **80**, 53 (1983).

- ⁵B. R. Ratna, R. Shashidar, and V. N. Raja, *Phys. Rev. Lett.* **55**, 1476 (1985).
- ⁶For a review of theory up to 1983, see J. Prost and P. Barois, *J. Chim. Phys.* **80**, 65 (1983).
- ⁷J. O. Indekeu and A. Nihat Berker, *Phys. Rev. A* **33**, 1158 (1986).
- ⁸C. R. Safinya, William A. Varady, L. Y. Chiang, and P. Dimon, *Phys. Rev. Lett.* **57**, 432 (1986).
- ⁹E. Fontes, P. A. Heiney, J. N. Haseltine, and A. B. Smith III, *J. Phys. (Paris)* **47**, 1533 (1986).
- ¹⁰K. K. Chan, P. S. Pershan, L. B. Sorensen, and F. Hardouin, *Phys. Rev. Lett.* **54**, 1694 (1986); C. W. Garland, C. Chiang, and F. Hardouin, *Liq. Cryst.* **1**, 81 (1986).
- ¹¹Nguyen Hun Tinh, G. Sigaud, M. F. Achard, H. Gasparoux, and F. Hardouin, in *Advances in Liquid Crystal Research and Applications*, edited by L. Bata (Pergamon, Oxford, 1980), p. 147.
- ¹²A. R. Kortan, H. von Kanel, R. J. Birgeneau, and J. D. Litster, *J. Phys. (Paris)* **45**, 529 (1984).
- ¹³F. Hardouin and A. M. Levelut, *J. Phys. (Paris)* **41**, 41 (1980); see also A. M. Levelut, R. J. Tarento, F. Hardouin, M. F. Achard, and G. Sigaud, *Phys. Rev. A* **24**, 2180 (1981).
- ¹⁴C. W. Garland, *Thermochim. Acta* **88**, 127 (1985); M. Meichle and C. W. Garland, *Phys. Rev. A* **27**, 2624 (1983).
- ¹⁵J. O. Indekeu, A. N. Berker, C. Chiang, and C. W. Garland, *Phys. Rev. A* **35**, 1371 (1987).
- ¹⁶J. C. LeGuillon and J. Zinn-Justin, *Phys. Rev. B* **21**, 3976 (1980).
- ¹⁷F. Hardouin, A. M. Levelut, and G. Sigaud, *J. Phys. (Paris)* **42**, 71 (1981).
- ¹⁸This was explicitly demonstrated for 40.7 in Ref. 1.
- ¹⁹This happens, for example, in the reentrant phase of monolayer Kr on graphite: E. D. Specht, M. Sutton, R. J. Birgeneau, D. E. Moncton, and P. M. Horn, *Phys. Rev. B* **30**, 1589 (1984).
- ²⁰L. J. Martinez-Miranda, A. R. Kortan, and R. J. Birgeneau, *Phys. Rev. Lett.* **56**, 2264 (1986).
- ²¹J.-C. Chen and T. C. Lubensky, *Phys. Rev. A* **14**, 1202 (1976).
- ²²C. R. Safinya, M. Kaplan, J. Als-Nielsen, R. J. Birgeneau, D. Davidov, J. D. Litster, D. L. Johnson, and M. E. Neubert, *Phys. Rev. B* **21**, 4149 (1980).
- ²³J. Als-Nielsen, R. J. Birgeneau, M. Kaplan, J. D. Litster, and C. R. Safinya, *Phys. Rev. Lett.* **39**, 352 (1977); **41**, 1626(E) (1978).
- ²⁴T. C. Lubensky and J. H. Chen, *Phys. Rev. B* **17**, 366 (1978); T. C. Lubensky, *J. Chim. Phys. (Paris)* **80**, 31 (1983); T. C. Lubensky, S. G. Dunn, and J. Isaacson, *Phys. Rev. Lett.* **22**, 1609 (1981).
- ²⁵P. G. de Gennes, *Solid State Commun.* **10**, 753 (1972); *Mol. Cryst. Liq. Cryst.* **21**, 49 (1973).
- ²⁶R. J. Birgeneau, C. W. Garland, G. B. Kasting, and B. M. Ocko, *Phys. Rev. B* **24**, 2624 (1981).
- ²⁷C. R. Safinya, R. J. Birgeneau, J. D. Litster, and M. E. Neubert, *Phys. Rev. Lett.* **47**, 668 (1981).